

Superconducting Diode Effect in Double Quantum Dot Device

Go Takeuchi and Mikio Eto

Faculty of Science and Technology, Keio University, Hiyoshi, Yokohama 223-8522, Japan

Superconducting diode effect (SDE) is theoretically examined in double quantum dot coupled to three superconducting leads, L , $R1$ and $R2$. Lead L is commonly connected to two quantum dots (QD1, QD2) while lead $R1$ ($R2$) is connected to QD1 (QD2) only. The phase differences φ_1 between leads L and $R1$ and φ_2 between leads L and $R2$ are tuned independently. The critical current into lead $R1$ depends on its direction unless $\varphi_2 = 0, \pi$, which is ascribable to the formation of Andreev molecule between the QDs. In the absence of electron-electron interaction U in the QDs, the spectrum of the Andreev bound states forms Dirac cones in the $\varphi_1 - \varphi_2$ plane if the energy levels in the QDs are tuned to the Fermi level in the leads. The SDE is enhanced to almost 30% when φ_2 is set to the value at the Dirac points. In the presence of U , the SDE is still observed when U is smaller than the superconducting energy gap in the leads. Our device should be one of the minimal models for the SDE since a similar device with a single QD does not show the SDE.

1. Introduction

Superconducting diode effect (SDE) has been studied intensively in various systems. The critical current can depend on the direction when both the time-reversal and spatial-inversion symmetries are broken. This effect could be applied to the dissipationless rectification in superconducting circuits, corresponding to pn junctions in traditional electronics. The SDE was observed, e. g., in a superconductor without the spatial-inversion symmetry in a magnetic field.¹⁾ Besides the intrinsic SDE in superconductors, the SDE was proposed in Josephson junction devices, so-called Josephson diode:²⁻⁴⁾ e.g., a semiconductor nanowire connected to two superconducting leads in the presence of spin-orbit interaction and Zeeman effect.^{5,6)} The Josephson diodes were realized using various materials,⁷⁻¹¹⁾ asymmetric superconducting quantum interference devices (SQUIDs),¹²⁻¹⁴⁾ multi-terminal devices,^{14,15)} etc.

Recently, Matsuo *et al.* observed the SDE in coupled Josephson junctions consisting of three superconducting leads: Each junction is connected to a common lead (lead L with superconducting phase ϕ_L) and another lead ($R1$ or $R2$ with ϕ_{R1} , ϕ_{R2} , respectively).^{16,17)} The

former gives rise to the coherent coupling between the junctions by the crossed Andreev reflection, in which an electron from a junction is reflected to a hole in another and vice versa, forming an “Andreev molecule.”^{18–22)} Then, the supercurrent to lead $R1$, I_1 , depends on not only $\varphi_1 = \phi_L - \phi_{R1}$ but also $\varphi_2 = \phi_L - \phi_{R2}$. Hence I_1 can be controlled by phase φ_2 in the nearby superconductor. For a given φ_2 ($\neq 0, \pi$), I_1 flows at $\varphi_1 = 0$ (anomalous Josephson effect)¹⁷⁾ and shows the SDE.¹⁶⁾ The SDE in this device does not require the spin-orbit interaction.

In this paper, we theoretically examine the SDE in three-terminal Josephson junctions using semiconductor quantum dots (QDs). The QDs are useful devices to examine various transport phenomena due to their tunability of various parameters, particularly discrete energy levels in the QDs. The QDs connected to the superconducting leads were studied in various contexts, including the competition between the Kondo effect and formation of the Andreev bound state, Yu-Shiba-Rusinov states (see Ref. 23 for the review), and observation of π -junction.²⁴⁾ The double quantum dot (DQD) was also studied,^{25–27)} for the application to the Cooper pair splitter to create an entangled pair of electrons,^{28,29)} observation of the poor man’s Majorana states as a minimal Kitaev chain,^{30–32)} etc.

We focus on the SDE in the DQD connected to three superconducting leads, depicted in Fig. 1(a), in a similar geometry to the device by Matsuo *et al.*^{16,17)} The Andreev molecule is formed between the QDs by the crossed Andreev reflection at lead L , which makes the supercurrent I_1 to lead $R1$ depend on both the phases φ_1 and φ_2 . We consider single energy levels in the QDs, assuming that the level spacing is larger than the superconducting gap Δ_0 in the leads. We also assume that their level broadening and Coulomb interaction U in the QDs are much smaller than Δ_0 , which simplifies the analysis of the supercurrent. The aim of this study is to elucidate the condition for the enhanced SDE.

First, we examine the case without U in the QDs. We calculate the energies of the Andreev bound states as a function of φ_1 and φ_2 by solving the Bogoliubov-de Gennes (BdG) equation. When the energy levels in the QDs are tuned to match the Fermi level in the leads, the energies become zero at some (φ_1, φ_2) and form Dirac cones around the points in the $\varphi_1 - \varphi_2$ plane. When φ_2 is fixed at the value of the Dirac points, the supercurrent I_1 shows a large SDE. Its efficiency can be around 30%. Second, we take U into account. Then, the groundstate is either spin singlet or doublet, depending on the phases φ_1 and φ_2 . The latter appears in the vicinity of the Dirac points in the case of $U = 0$. The supercurrent flows even in the doublet phase in our device. The transition between the spin states enhances the SDE.

Note that (i) the Dirac points were previously examined as Weyl singularities in the Josephson junctions with four or more superconducting leads.^{33–35)} In our device, the Dirac

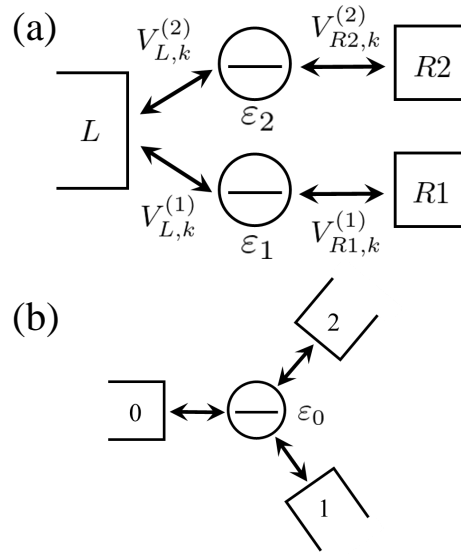


Fig. 1. (a) Our model of double quantum dot connected to three superconducting leads. QD1 (QD2) with energy level ε_1 (ε_2) is connected to leads L and $R1$ ($R2$). The strength of the tunnel couplings is characterized by the linewidth functions in Eqs. (5) and (6). The phase differences are given by $\varphi_1 = \phi_L - \phi_{R1}$ and $\varphi_2 = \phi_L - \phi_{R2}$, where ϕ_L , ϕ_{R1} , and ϕ_{R2} are the superconducting phases in respective leads. (b) Model of a single QD connected to three superconducting leads. This model is examined in Appendix C.

points can be realized by tuning the QDs. (ii) We find the anomalous Josephson effect and Dirac cones, but do not the SDE in a single QD connected to three superconducting leads, as depicted in Fig. 1(b). Hence, our model in Fig. 1(a) should be one of the minimal models for the SDE as long as simple QDs are considered without the chirality,³⁶⁾ spin-orbit interaction,³⁷⁾ etc.

This paper is organized as follows. We explain our model and calculation methods in the absence and presence of U in Sect. 2. Section 3 is devoted to the calculated results in the absence of U . We show that the spectrum of the Andreev bound states forms the Dirac cones in the $\varphi_1 - \varphi_2$ plan. The supercurrent to lead $R1$ and its SDE are enhanced when φ_2 is chosen to be the value at the Dirac points. In Sect. 4, we show the calculated results in the presence of U , showing a large SDE even in this case. We give the conclusions and discussion in Sect. 5. For comparison, we examine a single QD device in Fig. 1(b) in Appendix C.

2. Model and Calculation Method

2.1 Model and effective Hamiltonian

Our model of the DQD is depicted in Fig. 1(a). One of the QDs (QD1) is tunnel-coupled to superconducting leads L and $R1$ while the other (QD2) is to L and $R2$. The Hamiltonian is

given by

$$H^{\text{DQD}} = H_{\text{dots}} + H_S + H_T \quad (1)$$

with

$$H_{\text{dots}} = \sum_{j=1,2} \left(\sum_{\sigma} \varepsilon_j d_{j,\sigma}^{\dagger} d_{j,\sigma} + U n_{j\uparrow} n_{j\downarrow} \right), \quad (2)$$

$$H_S = \sum_{\alpha,k} \left[\sum_{\sigma} \varepsilon_k c_{\alpha,k\sigma}^{\dagger} c_{\alpha,k\sigma} - (\Delta_{\alpha} c_{\alpha,k\uparrow}^{\dagger} c_{\alpha,-k\downarrow}^{\dagger} + \text{h.c.}) \right], \quad (3)$$

$$H_T = \sum_{j=1,2} \sum_{k\sigma} \left[(V_{L,k}^{(j)} c_{L,k\sigma}^{\dagger} + V_{Rj,k}^{(j)} c_{Rj,k\sigma}^{\dagger}) d_{j,\sigma} + \text{h.c.} \right], \quad (4)$$

where $c_{\alpha,k\sigma}^{\dagger}$ and $c_{\alpha,k\sigma}$ are creation and annihilation operators for an electron in lead α ($= L, R1, R2$) with state k and spin σ , whereas $d_{j,\sigma}^{\dagger}$ and $d_{j,\sigma}$ are those in QD j with spin σ . $n_{j,\sigma} = d_{j,\sigma}^{\dagger} d_{j,\sigma}$ is the number operator in QD j with spin σ . In H_{dots} , ε_j is the energy level in QD j ($j = 1, 2$) and U is the electron-electron interaction in the QDs. The superconducting leads are described by H_S , where $\Delta_{\alpha} = \Delta_0 e^{i\phi_{\alpha}}$ with the s-wave superconducting gap Δ_0 and phase ϕ_{α} in lead α .

The tunnel couplings are given by H_T in which $V_{\alpha,k}^{(j)}$ are taken to be positive. The strength of the tunneling between QD j and lead Rj is characterized by the linewidth functions,

$$\Gamma_{Rj}(\varepsilon) = \pi \sum_k \left[V_{Rj,k}^{(j)} \right]^2 \delta(\varepsilon - \varepsilon_k) \quad (5)$$

($j = 1, 2$) while that between the DQD and lead L is by

$$\Gamma_{L,ij}(\varepsilon) = \pi \sum_k V_{L,k}^{(i)} V_{L,k}^{(j)} \delta(\varepsilon - \varepsilon_k) \quad (6)$$

in the form of 2×2 matrix ($i, j = 1, 2$). We assume their weak ε -dependence around the Fermi level E_F ($= 0$) and simply express Γ_{Rj} and $\Gamma_{L,ij}$ for $\varepsilon \simeq E_F$. The level broadening in QD j is given by $\Gamma_{Rj} + \Gamma_{L,jj}$. For the off-diagonal elements in Eq. (6), we introduce a parameter p ($0 \leq p \leq 1$) by

$$\Gamma_{L;12} = \Gamma_{L;21} = \sqrt{\Gamma_{L;11} \Gamma_{L;22}} p, \quad (7)$$

which determines the coherent coupling between the QDs through lead L .³⁸⁻⁴⁰⁾ p is identical to the overlap integral between the conduction modes coupled to QD1 and QD2 in the lead at the energy $\varepsilon \simeq E_F$.⁴¹⁾ In the case of single channel in the lead, $p = 1$ and the connection between the QDs is the maximal. With an increase in the channel number, p usually decreases. For $p = 0$, two QDs become independent of each other. In experiments, p is determined by the device structure.

In this paper, we restrict ourselves to the low-energy regime compared with the superconducting gap, assuming that $|\varepsilon_j|, U, \Gamma_{Rj}, \Gamma_{L;jj} \ll \Delta_0$ for $j = 1, 2$. By the Schrieffer-Wolff transformation,⁴²⁻⁴⁴⁾ we derive the effective Hamiltonian to the second-order of H_T ,

$$H_{\text{eff}}^{\text{DQD}} = H_{\text{dots}} + H_{\text{LAR}} + H_{\text{CAR}}. \quad (8)$$

Here,

$$H_{\text{LAR}} = \sum_{j=1,2} \left(\Gamma_{\text{LAR},j} d_{j\uparrow}^\dagger d_{j\downarrow}^\dagger + \text{h.c.} \right), \quad (9)$$

$$H_{\text{CAR}} = \Gamma_{\text{CAR}} \left(d_{1\uparrow}^\dagger d_{2\downarrow}^\dagger - d_{1\downarrow}^\dagger d_{2\uparrow}^\dagger \right) + \text{h.c.}, \quad (10)$$

where

$$\Gamma_{\text{LAR},j} = -\Gamma_{L;jj} e^{i\phi_L} - \Gamma_{Rj} e^{i\phi_{Rj}}, \quad (11)$$

$$\Gamma_{\text{CAR}} = -\sqrt{\Gamma_{L;11}\Gamma_{L;22}} p e^{i\phi_L}. \quad (12)$$

H_{LAR} represents the local Andreev reflection in which an electron in a QD is reflected to a hole in the same QD and vice versa at leads $R1, R2$, or L , whereas H_{CAR} represents the crossed Andreev reflection between the QDs at lead L . Note that the strength of the latter is proportional to the parameter p in Eq. (7).

2.2 Calculation method without U

We begin with the case of ‘‘one-body problem’’ in the absence of U . $H_{\text{eff}}^{\text{DQD}}$ in Eq. (8) is rewritten in the Nambu form as

$$H_{\text{eff}}^{\text{DQD}} = \begin{pmatrix} d_{1\uparrow}^\dagger, d_{1\downarrow}, d_{2\uparrow}^\dagger, d_{2\downarrow} \end{pmatrix} \begin{pmatrix} \varepsilon_1 & \Gamma_{\text{LAR},1} & 0 & \Gamma_{\text{CAR}} \\ \Gamma_{\text{LAR},1}^* & -\varepsilon_1 & \Gamma_{\text{CAR}}^* & 0 \\ 0 & \Gamma_{\text{CAR}} & \varepsilon_2 & \Gamma_{\text{LAR},2} \\ \Gamma_{\text{CAR}}^* & 0 & \Gamma_{\text{LAR},2}^* & -\varepsilon_2 \end{pmatrix} \begin{pmatrix} d_{1\uparrow} \\ d_{1\downarrow}^\dagger \\ d_{2\uparrow} \\ d_{2\downarrow}^\dagger \end{pmatrix} + \sum_{j=1,2} \varepsilon_j. \quad (13)$$

As shown in Appendix A, the BdG equation yields four eigenenergies, $\pm E_1, \pm E_2$ ($0 \leq E_1 \leq E_2$), corresponding to the Andreev bound states. After the Bogoliubov transformation, we obtain the groundstate energy,

$$E_{\text{GS}} = -\sum_{n=1,2} E_n + \sum_{j=1,2} \varepsilon_j. \quad (14)$$

Note that E_n is a function of the phase differences φ_1 and φ_2 , where

$$\varphi_j = \phi_L - \phi_{Rj} \quad (15)$$

for $j = 1, 2$. We denote the supercurrent into lead Rj by I_j ($j = 1, 2$), which is given by

$$I_j = \frac{2e}{\hbar} \frac{\partial E_{\text{GS}}}{\partial \varphi_j} \quad (16)$$

$$= -\frac{2e}{\hbar} \sum_{n=1,2} \frac{\partial E_n(\varphi_1, \varphi_2)}{\partial \varphi_j} \quad (17)$$

at temperature $T = 0$. This formula is derived using the Hellman-Feynman theorem.²³⁾

2.3 Calculation method with U

In the presence of U , we diagonalize the effective Hamiltonian $H_{\text{eff}}^{\text{DQD}}$ in Eq. (8) in the space of many-body states in the DQD. The space is divided into three subspaces with the total spin $S = 0, 1/2$, and 1.

In the subspace of spin singlet ($S = 0$), there are five states, $|0\rangle, |s\rangle, |1 \uparrow, 1 \downarrow\rangle, |2 \uparrow, 2 \downarrow\rangle$, and $|1 \uparrow, 1 \downarrow, 2 \uparrow, 2 \downarrow\rangle$, where $|0\rangle$ is the empty state in the DQD, $|j, \sigma\rangle = d_{j,\sigma}^\dagger |0\rangle$, and

$$|s\rangle = \frac{1}{\sqrt{2}} (|1 \uparrow, 2 \downarrow\rangle - |1 \downarrow, 2 \uparrow\rangle). \quad (18)$$

Using these states as a basis set, the Hamiltonian is represented by Eq. (B·1) in Appendix B. Its diagonalization yields the energies of the many-body Andreev bound states. The lowest one is denoted by E_{singlet} .

The subspace of spin doublet ($S = 1/2$) consists of the space with $S_z = 1/2$ and that with $S_z = -1/2$. Each space includes four states; $|1 \uparrow\rangle, |2 \uparrow\rangle, |1 \uparrow, 2 \uparrow, 2 \downarrow\rangle, |1 \uparrow, 1 \downarrow, 2 \uparrow\rangle$ in the former and $|1 \downarrow\rangle, |2 \downarrow\rangle, |1 \downarrow, 2 \uparrow, 2 \downarrow\rangle, |1 \uparrow, 1 \downarrow, 2 \downarrow\rangle$ in the latter. The diagonalization of the representation matrix in Eq. (B·2) gives the lowest energy, E_{doublet} , which is doubly degenerate with $S_z = \pm 1/2$.

Finally, three spin-triplet states, $|1 \uparrow, 2 \uparrow\rangle$,

$$|t\rangle = \frac{1}{\sqrt{2}} (|1 \uparrow, 2 \downarrow\rangle + |1 \downarrow, 2 \uparrow\rangle), \quad (19)$$

and $|1 \downarrow, 2 \downarrow\rangle$, are already the eigenstates of $H_{\text{eff}}^{\text{DQD}}$. The eigenenergies are $\varepsilon_1 + \varepsilon_2 \equiv E_{\text{triplet}}$.

The groundstate energy E_{GS} is determined by the minimum among E_{singlet} , E_{doublet} , and E_{triplet} . Note that both E_{singlet} and E_{doublet} depend on the phase differences φ_1 and φ_2 in Eq. (15) while E_{triplet} does not.

The supercurrent is given by the formula in Eq. (16). It flows in the spin-singlet or doublet phases and does not in the triplet phase.

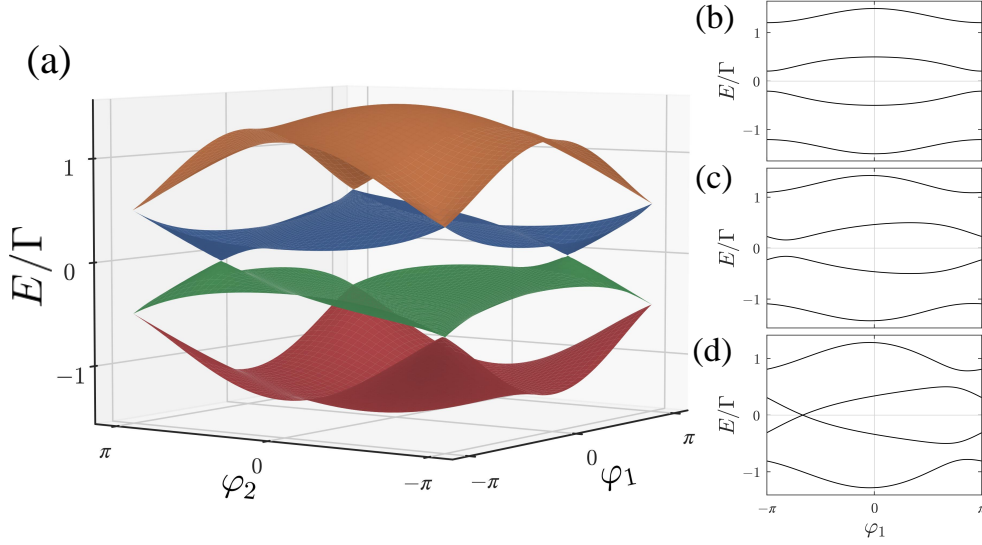


Fig. 2. (Color online) Energies of Andreev bound states, $\pm E_1$ and $\pm E_2$ ($0 \leq E_1 \leq E_2$), in the model in Fig. 1(a) with $U = 0$, $\varepsilon_1 = \varepsilon_2 = 0$, $\Gamma_{L;11} = \Gamma_{R1} = \Gamma_{L;22} = \Gamma_{R2} = \Gamma/2$, and $p = 1$, where Γ is the level broadening in the QDs. (a) The energies plotted in the $\varphi_1 - \varphi_2$ plane. E_1 and $-E_1$ form the Dirac cones around the zero points at $(\varphi_1, \varphi_2) = \pm(2\pi/3, -2\pi/3)$. (b)–(d) Cross sections of panel (a) at (b) $\varphi_2 = 0$, (c) $\pi/3$, and (d) $2\pi/3$.

3. Calculated Results in the Absence of U

In this section, we discuss the case of $U = 0$. First, we examine the spectrum of the Andreev bound states. Figure 2(a) depicts $\pm E_1$ and $\pm E_2$ ($0 \leq E_1 \leq E_2$) in the $\varphi_1 - \varphi_2$ plane. We match the energy levels in the QDs to the Fermi level, $\varepsilon_1 = \varepsilon_2 = 0$, and set $\Gamma_{L;11} = \Gamma_{R1} = \Gamma_{L;22} = \Gamma_{R2} = \Gamma/2$ and $p = 1$, where Γ is the level broadening in the QDs. In this case, $E_1 = 0$ at $(\varphi_1, \varphi_2) = \pm(2\pi/3, -2\pi/3)$, which is derived in Appendix A. The energies of $\pm E_1(\varphi_1, \varphi_2)$ form a “Dirac cone” around these zero-points.

Note that $E_n(-\varphi_1, \varphi_2) \neq E_n(\varphi_1, \varphi_2)$ unless $\varphi_2 = 0$ or π although the identity of $E_n(-\varphi_1, -\varphi_2) = E_n(\varphi_1, \varphi_2)$ always holds by the time-reversal relation. Figures 2(b)–(d) depict the cross sections of Fig. 2(a) at (b) $\varphi_2 = 0$, (c) $\pi/3$, and (d) $2\pi/3$. The energies $\pm E_1$ and $\pm E_2$ are even functions of φ_1 at $\varphi_2 = 0$, whereas they are asymmetric about $\varphi_1 = 0$ at $\varphi_2 \neq 0$. E_1 has a zero point at $\varphi_2 = 2\pi/3$, corresponding to the Dirac points.

We calculate the supercurrent into lead $R1$, I_1 , using the formula in Eq. (17). Figure 3 shows the current as a function of φ_1 when φ_2 is fixed at 0 , $\pi/3$, $2\pi/3$, and $3\pi/4$. When $\varphi_2 = 0$, I_1 is positive (negative) at $0 < \varphi_1 < \pi$ ($-\pi < \varphi_1 < 0$). I_1 is an odd function of φ_1 , and hence $I_1 = 0$ at $\varphi_1 = 0$. When $\varphi_2 \neq 0$ ($0 < \varphi_2 < \pi$), however, I_1 is not an odd function of φ_1 . I_1 flows at $\varphi_1 = 0$, indicating an anomalous Josephson effect. The behavior of I_1 changes gradually with φ_2 in the positive region of φ_1 , whereas it changes drastically with φ_2 in the

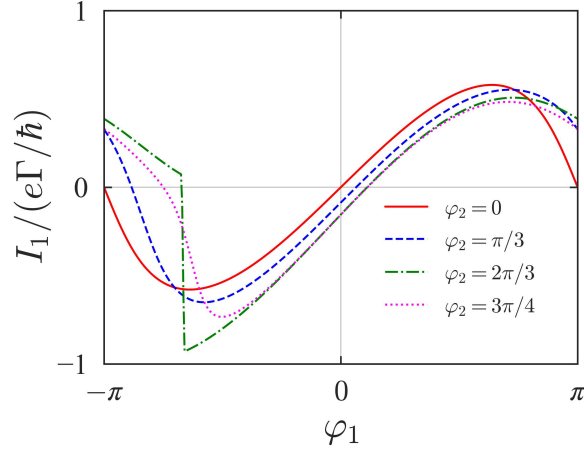


Fig. 3. (Color online) Supercurrent I_1 to lead $R1$ as a function of φ_1 , in the model in Fig. 1(a) with $U = 0$, when φ_2 is fixed at 0 (solid line), $\pi/3$ (broken line), $2\pi/3$ (dash-dotted line), and $3\pi/4$ (dotted line). $\varepsilon_1 = \varepsilon_2 = 0$, $\Gamma_{L;11} = \Gamma_{R1} = \Gamma_{L;22} = \Gamma_{R2} \equiv \Gamma/2$, and $p = 1$.

negative region of φ_1 . Particularly, I_1 shows a step at $\varphi_1 = -2\pi/3$ when $\varphi_2 = 2\pi/3$. This is due to the Dirac point since $\partial E_1/\partial\varphi_1 < 0$ (> 0) at $\varphi_1 = -2\pi/3 - 0$ ($+0$).

In Fig. 3, we observe that the maximum of $|I_1|$ is different in the positive and negative directions when $\varphi_2 \neq 0$. If the critical currents are denoted by $I_c^\pm(\varphi_2) = \max_{\varphi_1}[\pm I_1(\varphi_1, \varphi_2)]$, $I_c^- = I_c^+$ for $\varphi_2 = 0$ and $I_c^- > I_c^+$ for $0 < \varphi_2 < \pi$. This diode effect is the maximal when $\varphi_2 = 2\pi/3$, the value of the Dirac point. The mechanism is as follows. E_1 is very steep at the Dirac point and thus $|\partial E_1/\partial\varphi_1|$ becomes large there [$\partial E_1/\partial\varphi_1 = \mp\Gamma/4$, see Appendix A]. Since $\partial E_2/\partial\varphi_1 > 0$ around the point, the step of I_1 is shifted in the negative direction by Eq. (17), which results in a large I_c^- . On the other hand, I_1 takes the maximum in the positive region of φ_1 . I_c^+ changes slowly with φ_2 , as seen above. In consequence, the SDE is the maximal at $\varphi_2 = 2\pi/3$. It should be mentioned that the Dirac cone does not give rise to the SDE by itself although it is anisotropic, as shown in Fig. A.1. This is because $\partial E_1/\partial\varphi_1$ is the same in magnitude at $\varphi_1 = -2\pi/3 \pm 0$, as discussed in Appendix A.

For the quantitative discussion on the SDE, we define its efficiency by

$$\eta(\varphi_2) = \frac{I_c^+ - I_c^-}{I_c^+ + I_c^-}. \quad (20)$$

The time-reversal relation leads to the identities, $I_c^\pm(-\varphi_2) = I_c^\mp(\varphi_2)$ and thus $\eta(-\varphi_2) = -\eta(\varphi_2)$. In Fig. 4, we plot (a) the critical current into lead $R1$, $I_c^\pm(\varphi_2)$, and (b) the diode efficiency $\eta(\varphi_2)$. Both I_c^\pm and $\pm\eta$ are enhanced to the maximum at $\varphi_2 = \mp 2\pi/3$, the values at the Dirac points. The efficiency can reach almost ± 0.3 there. This is the main result in this paper.

We discuss the generality of the enhancement of the SDE. In Fig. 5, we plot $I_c^-(\varphi_2)$ and

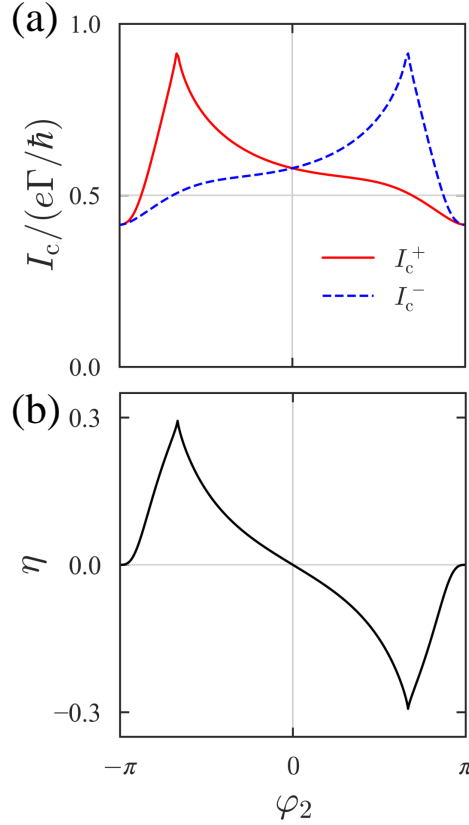


Fig. 4. (Color online) (a) Critical current I_c^\pm to lead $R1$ and (b) its diode efficiency η as functions of φ_2 , in the model in Fig. 1(a) with $U = 0$. The critical current I_c^+ (I_c^-) in the positive (negative) direction is depicted by solid (broken) line in panel (a). $\varepsilon_1 = \varepsilon_2 = 0$, $\Gamma_{L;11} = \Gamma_{R1} = \Gamma_{L;22} = \Gamma_{R2} \equiv \Gamma/2$, and $p = 1$.

$\eta(\varphi_2)$ when (a) $\varepsilon_1 = \varepsilon_2 = 0$ with various p , (b) $\varepsilon_1 = -\varepsilon_2 \equiv \varepsilon_0$ with $p = 1$, and (c) $\varepsilon_1 = \varepsilon_2 \equiv \varepsilon_0$ with $p = 1$. We choose $\Gamma_{L;11} = \Gamma_{R1} = \Gamma_{L;22} = \Gamma_{R2} = \Gamma/2$. [We do not plot $I_c^+(\varphi_2)$ since it is given by $I_c^-(-\varphi_2)$.]

With decreasing p , the crossed Andreev reflection becomes less effective [see Γ_{CAR} in Eq. (12)] and thus the diode efficiency decreases, as shown in Fig. 5(a). With $p = 0.5$, we still observe the enhanced critical current and $\eta \approx 0.15$ around the Dirac point. Note that the position of the Dirac points moves with p , following Eqs. (A·9) and (A·10) in Appendix A, where $I_c^-(\eta)$ has a cusp (cusps).

When $\varepsilon_1 = -\varepsilon_2 \equiv \varepsilon_0$, the Dirac points exist when $|\varepsilon_0| < \Gamma p/2$ (Appendix A). As seen in Fig. 5(b), I_c^- (or I_c^+) and $|\eta|$ are the largest at the points unless $|\varepsilon_0|/\Gamma$ is too large.⁴⁵⁾ For $|\varepsilon_0|/\Gamma = 1/2$, we find an enhancement of I_c^- and $|\eta|$ without a cusp although the Dirac point just disappears.

When $\varepsilon_1 = \varepsilon_2 \equiv \varepsilon_0 \neq 0$, the Dirac points are absent. We still observe the SDE with

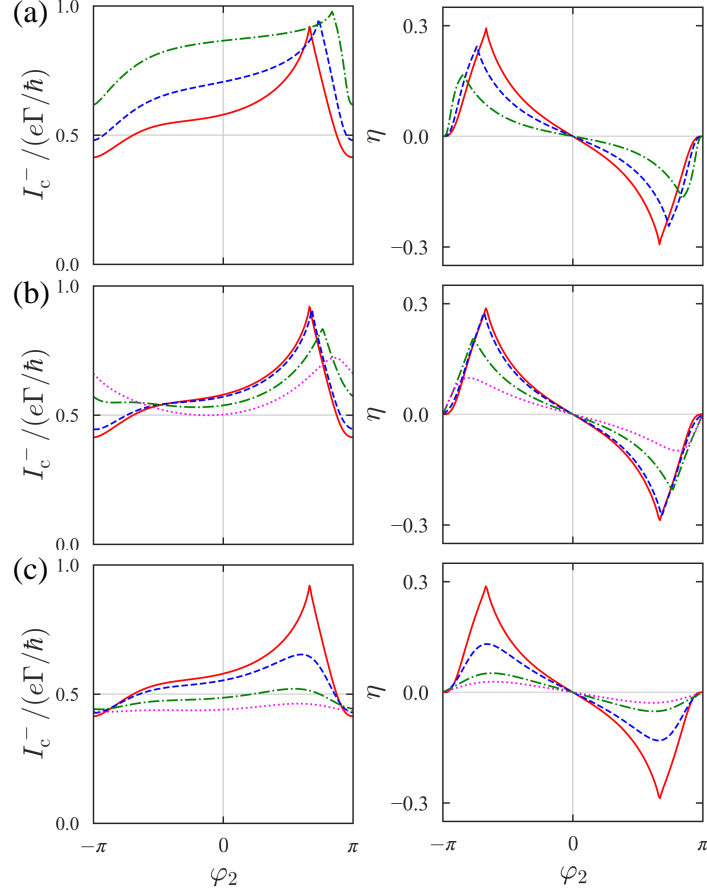


Fig. 5. (Color online) Critical current I_c^- to lead $R1$ (left panels) and its diode efficiency η (right panels) as functions of φ_2 , in the model in Fig. 1(a) with $U = 0$. $\Gamma_{L;11} = \Gamma_{R1} = \Gamma_{L;22} = \Gamma_{R2} \equiv \Gamma/2$. (a) $\varepsilon_1 = \varepsilon_2 = 0$ and $p = 1$ (solid line), 0.8 (broken line), and 0.5 (dash-dotted line). (b) [(c)] $\varepsilon_1 = -\varepsilon_2 \equiv \varepsilon_0$ [$\varepsilon_1 = \varepsilon_2 \equiv \varepsilon_0$] with $p = 1$. $\varepsilon_0/\Gamma = 0$ (solid line), 0.15 (broken line), 0.35 (dash-dotted line), and 0.5 (dotted line).

$|\eta| \simeq 0.13$ for $\varepsilon_0/\Gamma = 0.15$ in Fig. 5(c). The SDE becomes less prominent for $\varepsilon_0/\Gamma \gtrsim 0.35$.

We comment on the existence of Dirac points with arbitrary values of $\Gamma_{L;11}$, Γ_{R1} , $\Gamma_{L;22}$, and Γ_{R2} . When $\varepsilon_1 = \varepsilon_2 = 0$, the Dirac points exist if $b = 0$ in Eq. (A·12) at some (φ_1, φ_2) . This condition is usually satisfied when Γ 's are in the same order of magnitude. In the case of $p = 1$, the condition is given by a triangle inequality in Eq. (A·13).

In summary, the SDE of the supercurrent to lead $R1$ is largely enhanced when φ_2 is set to the value at the Dirac points when they are present. A large SDE is still observable when the Dirac points are absent and thus the Dirac cone becomes the spectrum of a “massive particle.” Around the dips of $E_1(\varphi_1, \varphi_2)$, $\partial E_1/\partial \varphi_1$ takes large values in magnitude with both positive and negative signs. This enhances the critical current I_c^- (I_c^+) if $\partial E_2/\partial \varphi_1 > 0$ (< 0) around the dips of E_1 , which results in a large SDE.

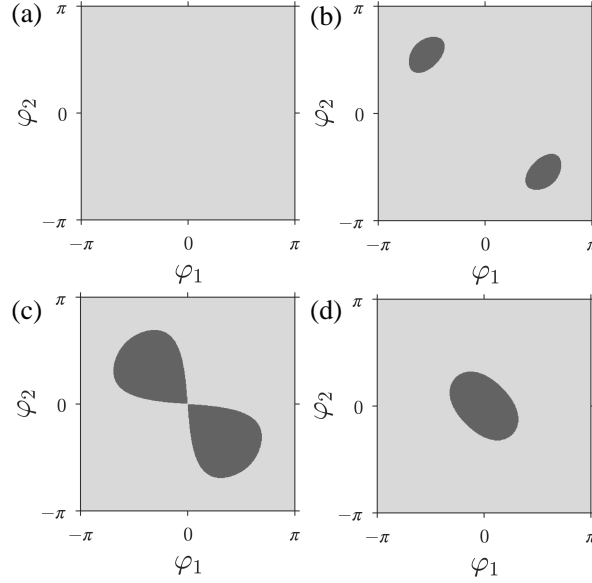


Fig. 6. Spin of the groundstate in the model in Fig. 1(a). The spin-singlet (doublet) regions are indicated by light gray (dark gray) in the $\varphi_1 - \varphi_2$ plane. $\varepsilon_1 = \varepsilon_2 = -U/2$, $\Gamma_{L;11} = \Gamma_{R1} = \Gamma_{L;22} = \Gamma_{R2} \equiv \Gamma/2$, and $p = 1$. (a) $U/\Gamma = 0$, (b) 0.5, (c) 1, and (d) 2.

4. Calculated Results in the Presence of U

In the presence of U , we choose the energy levels in the QDs to satisfy the electron-hole symmetry, $\varepsilon_1 = \varepsilon_2 = -U/2$. We set $\Gamma_{L;11} = \Gamma_{R1} = \Gamma_{L;22} = \Gamma_{R2} = \Gamma/2$ and $p = 1$, with Γ being the level broadening in the QDs.

The groundstate is either spin singlet or doublet in the presence of U . In Fig. 6, we plot the phase diagram in the $\varphi_1 - \varphi_2$ plane for (a) $U/\Gamma = 0$, (b) 0.5, (c) 1, and (d) 2. When $U = 0$, the spin-singlet phase is always realized (singlet and doublet energies are degenerate just at the Dirac points). For small U/Γ , the doublet phase appears around the Dirac points in the case of $U = 0$. The regions of the doublet phase are extended with an increase in U and merge at $U/\Gamma \geq 1$. With increasing U beyond $U/\Gamma = 2$, the region is shrunk and finally disappears. (When $U/\Gamma \gg 1$, $E_{\text{singlet}} \lesssim E_{\text{triplet}} < E_{\text{doublet}}$. The groundstate is almost $|s\rangle$ in Eq. (18) in which each QD accommodates one electron. Small amplitudes of the other components, such as $|0\rangle$ and $|1 \uparrow, 1 \downarrow\rangle$, weaken the Andreev reflection and reduce the supercurrent.)

In Fig. 7, we plot the energy of the many-body groundstate, E_{GS} , and supercurrent to lead $R1$, I_1 , as functions of φ_1 when φ_2 is fixed at the maximum of $-\eta$, as discussed below. The values of U/Γ are the same as in Fig. 6. When $U = 0$, I_1 shows a step at $\varphi_1 = -2\pi/3$, where E_{GS} has a kink, corresponding to the Dirac point, discussed in the previous section. When $U \neq 0$, I_1 shows two steps at the kinks of E_{GS} , where the groundstate changes between spin

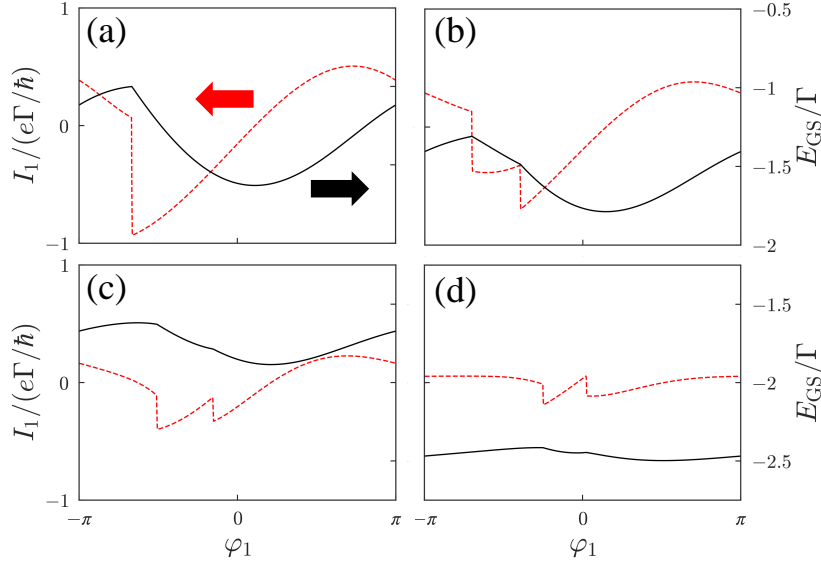


Fig. 7. (Color online) Supercurrent I_1 to lead $R1$ (broken line) and groundstate energy E_{GS} (solid line), as functions of φ_1 with a given φ_2 , in the model in Fig. 1(a). $\varepsilon_1 = \varepsilon_2 = -U/2$, $\Gamma_{L;11} = \Gamma_{R1} = \Gamma_{L;22} = \Gamma_{R2} \equiv \Gamma/2$, and $p = 1$. (a) $U/\Gamma = 0$, (b) 0.5, (c) 1, and (d) 2. φ_2 is chosen at the maximum of $-\eta(\varphi_2)$ in Fig. 8: (a) $\varphi_2 = 2\pi/3$, (b) 0.55π , (c) 0.63π , and (d) 0.28π . At the kinks of E_{GS} , the spin state changes in the groundstate, where I_1 shows a step.

singlet and doublet. Note that the supercurrent flows even in the doublet phase in our device, as noted in Sect. 2.3. At one of the steps, $-I_1$ takes the maximum, which results in a large critical current I_c^- in the negative direction.

Finally, Fig. 8 indicates the diode efficiency of the supercurrent I_1 as a function of φ_2 . The enhanced SDE is still seen in the presence of U . The maximum of $|\eta|$ is almost the same for $U/\Gamma = 0 \sim 1$. Although $|\eta|$ is larger than 50% when $U/\Gamma = 2$, the absolute value of the supercurrent I_1 is not large in Fig. 7(d). For $U/\Gamma > 2$, both the critical current and the SDE decrease with increasing U .

In this section, we have shown the calculated results only when $\Gamma_{L;11} = \Gamma_{R1} = \Gamma_{L;22} = \Gamma_{R2}$ and $p = 1$. When $\Gamma_{L;11}$, Γ_{R1} , $\Gamma_{L;22}$, and Γ_{R2} are not identical but are in the same order of magnitude, we find almost the same enhancement of the SDE as in Fig. 8 if $p = 1$. With a decrease in the parameter p , the efficiency $|\eta|$ decreases. For $p = 0.5$, we still observe $|\eta| \simeq 20\%$.

5. Conclusions and Discussion

We have theoretically examined the SDE in the DQD connected to three superconducting leads, depicted in Fig. 1(a). The geometry of this device is similar to that by Matsuo *et al.*^{16,17)}

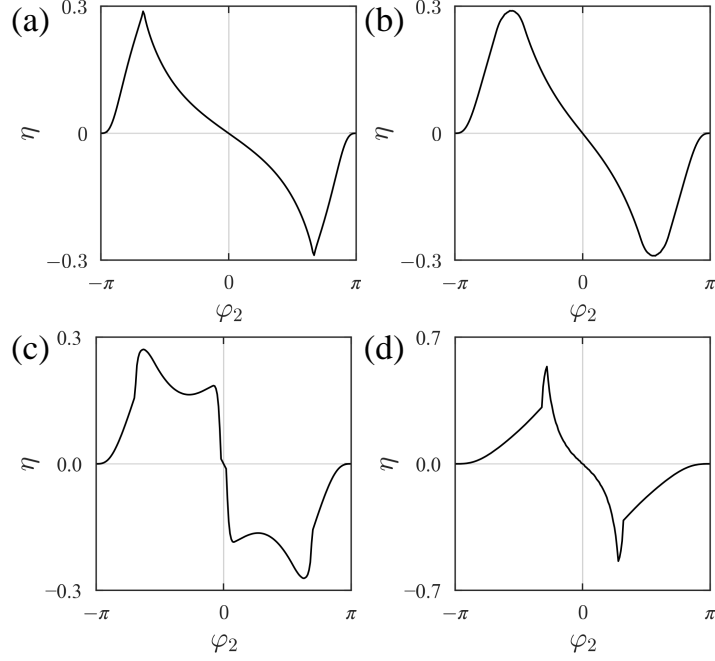


Fig. 8. Diode efficiency η of the supercurrent to lead $R1$ as a function of φ_2 , in the model in Fig. 1(a). $\varepsilon_1 = \varepsilon_2 = -U/2$, $\Gamma_{L,11} = \Gamma_{R1} = \Gamma_{L,22} = \Gamma_{R2} \equiv \Gamma/2$, and $p = 1$. (a) $U/\Gamma = 0$, (b) 0.5, (c) 1, and (d) 2.

The crossed Andreev reflection at lead L results in the formation of the Andreev molecule between the QDs, which makes the supercurrent to lead $R1$, I_1 , depend on both the phase differences $\varphi_1 = \varphi_L - \varphi_{R1}$ and $\varphi_2 = \varphi_L - \varphi_{R2}$. We have formulated the energies of the Andreev bound states and evaluated the supercurrent I_1 in both the cases of $U = 0$ and $U \neq 0$ in the QDs.

In the absence of U , we have obtained the Andreev bound states ($\pm E_1, \pm E_2$ with $0 \leq E_1 \leq E_2$) by solving the BdG equation. When the energy levels in the QDs are tuned to match the Fermi level in the leads, the energies $\pm E_1$ form Dirac cones in the $\varphi_1 - \varphi_2$ plane. When φ_2 is fixed at the value of the Dirac points, one of the critical currents I_c^\pm in the positive or negative directions is enhanced, which leads to a large SDE. Its efficiency can be around 30%. In the absence of Dirac points, an enhanced SDE is still observable around the dips of E_1 .

In the presence of U , we have diagonalized the Hamiltonian in the space of many-body states in the DQD. We have found that the groundstate is either spin singlet or doublet, depending on φ_1 and φ_2 . The supercurrent flows even in the doublet phase in our device. The transition between the singlet and doublet phases enhances the SDE. Its efficiency is almost the same as in the case of $U = 0$.

For comparison, we examine a single QD connected to three superconducting leads, depicted in Fig. 1(b), in Appendix C. In the absence of U , (i) the groundstate energy takes the

minimum at $\varphi_1 = \Phi$ in Eqs. (C·8) and (C·9) for a given φ_2 . Unless $\varphi_2 = 0$ or π , $\Phi \neq 0, \pi$ and hence I_1 flows at $\varphi_1 = 0$ (anomalous Josephson effect). (ii) When the energy level ε_0 in the QD is tuned to the Fermi level in the leads, the energies of the Andreev bound states have zero points if Γ_0, Γ_1 , and Γ_2 satisfy the condition in Eq. (C·10). Then, the Dirac cones appear in the $\varphi_1 - \varphi_2$ plane. However, (iii) the device of single QD does not show the SDE. At least two QDs or two levels in a single QD are required for the SDE as long as simple QDs are considered without the spin-orbit interaction, etc.^{36,37} Thus, our device in Fig. 1(a) should be one of the minimal models to show the SDE. (iv) In the presence of U , we set $\varepsilon_0 = -U/2$. Then, the groundstate is spin singlet or doublet. The supercurrent I_1 is equivalent to that with $U = 0$ in the singlet phase, whereas $I_1 = 0$ in the doublet phase.

In this paper, we have examined the effective Hamiltonian in Eq. (8), which is obtained by the Schrieffer-Wolff transformation to the second-order of the tunnel Hamiltonian H_T . Thus, our study is only applicable to the low-energy regime compared with the superconducting gap; $|\varepsilon_j|, U, \Gamma_{Rj}, \Gamma_{L;jj} \ll \Delta_0$ for $j = 1, 2$. Otherwise, the higher-order terms with respect to H_T have to be taken into account as in, e.g., Refs. 46 and 47 for a single QD.

Finally, we stress the merits of the QD device. The tunability of the energy levels in the QDs enables the investigation of the spectrum of the Andreev bound states in detail, artificial creation of the Dirac cones in the $\varphi_1 - \varphi_2$ plane, and the realization of a large SDE. This should lead to the deeper understanding of the physics of Andreev bound states and molecules.

Acknowledgments

We appreciate fruitful discussions with Dr. Rui Sakano. This work was partially supported by JSPS KAKENHI Grant Number JP20K03807.

Appendix A: Bogoliubov Transformation and Dirac Points in the Absence of U

A.1 Bogoliubov transformation

In the absence of U , the effective Hamiltonian is given by Eq. (13), or

$$H_{\text{eff}}^{\text{DQD}} = \left(d_{1\uparrow}^\dagger, d_{1\downarrow}, d_{2\uparrow}^\dagger, d_{2\downarrow} \right) \mathcal{H} \begin{pmatrix} d_{1\uparrow} \\ d_{1\downarrow}^\dagger \\ d_{2\uparrow} \\ d_{2\downarrow}^\dagger \end{pmatrix} + \sum_{j=1,2} \varepsilon_j \quad (\text{A}\cdot 1)$$

with

$$\mathcal{H} = \begin{pmatrix} \varepsilon_1 & \Gamma_{\text{LAR},1} & 0 & \Gamma_{\text{CAR}} \\ \Gamma_{\text{LAR},1}^* & -\varepsilon_1 & \Gamma_{\text{CAR}}^* & 0 \\ 0 & \Gamma_{\text{CAR}} & \varepsilon_2 & \Gamma_{\text{LAR},2} \\ \Gamma_{\text{CAR}}^* & 0 & \Gamma_{\text{LAR},2}^* & -\varepsilon_2 \end{pmatrix}. \quad (\text{A}\cdot 2)$$

The solution of the BdG equation, $\mathcal{H}\mathbf{u} = E\mathbf{u}$, is given by $E = \pm E_1, \pm E_2$ ($0 \leq E_1 \leq E_2$), where

$$E_{1,2} = \sqrt{\frac{a \mp \sqrt{a^2 - 4b}}{2}}, \quad (\text{A}\cdot 3)$$

with

$$a = \varepsilon_1^2 + \varepsilon_2^2 + |\Gamma_{\text{LAR},1}|^2 + |\Gamma_{\text{LAR},2}|^2 + 2|\Gamma_{\text{CAR}}|^2, \quad (\text{A}\cdot 4)$$

$$b = \varepsilon_1^2 \varepsilon_2^2 + |\Gamma_{\text{LAR},2}|^2 \varepsilon_1^2 + |\Gamma_{\text{LAR},1}|^2 \varepsilon_2^2 + 2\varepsilon_1 \varepsilon_2 |\Gamma_{\text{CAR}}|^2 \\ + |\Gamma_{\text{CAR}}|^4 + |\Gamma_{\text{LAR},1}|^2 |\Gamma_{\text{LAR},2}|^2 - \left(\Gamma_{\text{CAR}}^2 \Gamma_{\text{LAR},1}^* \Gamma_{\text{LAR},2} + \text{c.c.} \right). \quad (\text{A}\cdot 5)$$

When $\mathbf{u}_n = (u_1, v_1, u_2, v_2)^T$ is the eigenfunction corresponding to E_n , $\tilde{\mathbf{u}}_n = (-v_1^*, u_1^*, -v_2^*, u_2^*)^T$ is that to $-E_n$. The unitary matrix, $U = (\mathbf{u}_1, \tilde{\mathbf{u}}_1, \mathbf{u}_2, \tilde{\mathbf{u}}_2)$, satisfies $P^\dagger \tilde{H} P = \text{diag}(E_1, -E_1, E_2, -E_2)$. Thus the Bogoliubov transformation

$$\begin{pmatrix} d_{1\uparrow} \\ d_{1\downarrow}^\dagger \\ d_{2\uparrow} \\ d_{2\downarrow}^\dagger \end{pmatrix} = P \begin{pmatrix} \gamma_{1\uparrow} \\ \gamma_{1\downarrow}^\dagger \\ \gamma_{2\uparrow} \\ \gamma_{2\downarrow}^\dagger \end{pmatrix} \quad (\text{A}\cdot 6)$$

changes the Hamiltonian in Eq. (A.1) to

$$H_{\text{eff}}^{\text{DQD}} = \sum_{\sigma=\uparrow,\downarrow} \left(E_1 \gamma_{1\sigma}^\dagger \gamma_{1\sigma} + E_2 \gamma_{2\sigma}^\dagger \gamma_{2\sigma} \right) - \sum_{n=1,2} E_n + \sum_{j=1,2} \varepsilon_j. \quad (\text{A}\cdot 7)$$

As a result, the groundstate energy is given by Eq. (14).

Alternatively, E_1 and E_2 can be calculated using the retarded Green's function in the Nambu form of 4×4 matrix.²⁶⁾ Its trace possesses the poles at $E = \pm E_1 - i\delta$ and $\pm E_2 - i\delta$ with an infinitesimally small δ .

A.2 Dirac points

Consider zero points of the spectrum of Andreev bound states. The condition for $E_1 = 0$ is given by $b = 0$ in Eq. (A.5).

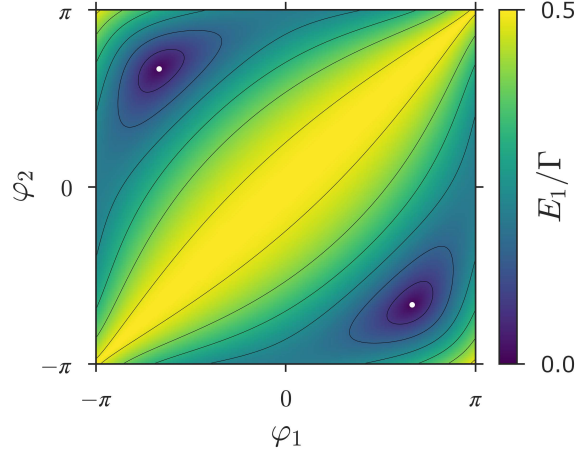


Fig. A.1. (Color online) Contour lines of the energy E_1 of Andreev bound state in the $\varphi_1 - \varphi_2$ plane, in the model in Fig. 1(a) with $U = 0$, $\varepsilon_1 = \varepsilon_2 = 0$, $\Gamma_{L;11} = \Gamma_{R1} = \Gamma_{L;22} = \Gamma_{R2} \equiv \Gamma/2$, and $p = 1$. E_1 forms anisotropic Dirac cones around the zero points, $\pm(2\pi/3, -2\pi/3)$, indicated by white dots.

First, we examine the case of $\Gamma_{L;11} = \Gamma_{R1} = \Gamma_{L;22} = \Gamma_{R2} \equiv \Gamma/2$. Then,

$$b = \varepsilon_1^2 \varepsilon_2^2 + \frac{1}{2} \Gamma^2 (1 + \cos \varphi_2) \varepsilon_1^2 + \frac{1}{2} \Gamma^2 (1 + \cos \varphi_1) \varepsilon_2^2 + \frac{1}{2} \Gamma^2 p^2 \varepsilon_1 \varepsilon_2 + \frac{\Gamma^4}{16} \left[4 + p^4 - 2p^2 + (4 - 2p^2)(\cos \varphi_1 + \cos \varphi_2) + 4 \cos \varphi_1 \cos \varphi_2 - 2p^2 \cos(\varphi_1 + \varphi_2) \right]. \quad (\text{A}\cdot 8)$$

Here, we discuss a situation of $|\varepsilon_1| = |\varepsilon_2|$. In this case, the solutions of $b = 0$ exist when $\varepsilon_1 = -\varepsilon_2 \equiv \varepsilon_0$ and $|\varepsilon_0| < \Gamma p/2$. There are two solutions, $(\varphi_1, \varphi_2) = (\varphi_1^{(0)}, \varphi_2^{(0)})$, where

$$\cos \varphi_1^{(0)} = -1 + \frac{1}{2} p^2 - \frac{2\varepsilon_0^2}{\Gamma^2}, \quad (\text{A}\cdot 9)$$

$$\varphi_2^{(0)} = -\varphi_1^{(0)}. \quad (\text{A}\cdot 10)$$

Around these zero-points, $E_1(\varphi_1, \varphi_2)$ behaves as

$$E_1(\varphi_1^{(0)} + \delta\varphi_1, \varphi_2^{(0)} + \delta\varphi_2) = \frac{\Gamma}{4} \sqrt{1 + \left[p^2 \left(\frac{4\varepsilon_0^2}{\Gamma^2 p^2} \right)^2 + (4 - 2p^2) \left(\frac{4\varepsilon_0^2}{\Gamma^2 p^2} \right) + p^2 - 2 \right] \cos \theta \sin \theta \delta\varphi}, \quad (\text{A}\cdot 11)$$

where $\delta\varphi_1 = \delta\varphi \cos \theta$ and $\delta\varphi_2 = \delta\varphi \sin \theta$ ($\delta\varphi > 0$). This indicates an anisotropic Dirac cone.

When $p = 1$ and $\varepsilon_0 = 0$, $E_1(\varphi_1, \varphi_2)$ is shown in Fig. A.1 by the contour lines. Equations (A.9)–(A.11) yield $\varphi_1^{(0)} = -\varphi_2^{(0)} = \pm 2\pi/3$ and $E_1 \simeq (\Gamma/4) \sqrt{1 - \cos \theta \sin \theta} \delta\varphi$ around the Dirac points. When $\delta\varphi_2 = 0$ ($\theta = 0, \pi$), $E_1(\varphi_1^{(0)} \pm \delta\varphi, \varphi_2^{(0)}) \simeq (\Gamma/4) \delta\varphi$, and thus $\partial E_1 / \partial \varphi_1 = \pm \Gamma/4$ at $\varphi_1 = \varphi_1^{(0)} \pm 0$ and $\varphi_2 = \varphi_2^{(0)}$.

Second, we derive the condition for the existence of Dirac points when $\varepsilon_1 = \varepsilon_2 = 0$ with arbitrary $\Gamma_{L;11}$, Γ_{R1} , $\Gamma_{L;22}$, Γ_{R2} , and p . Then,

$$\begin{aligned} b &= \left| \Gamma_{\text{CAR}}^2 - \Gamma_{\text{LAR},1} \Gamma_{\text{LAR},2} \right|^2 \\ &= \left| \Gamma_{L;11} \Gamma_{L;22} (1 - p^2) + \Gamma_{R1} \Gamma_{L;22} e^{i\varphi_1} + \Gamma_{L;11} \Gamma_{R2} e^{i\varphi_2} + \Gamma_{R1} \Gamma_{R2} e^{i(\varphi_1 + \varphi_2)} \right|^2. \end{aligned} \quad (\text{A}\cdot 12)$$

The Dirac points exist when $b = 0$ at some (φ_1, φ_2) . For $p = 1$, the solutions exist when $\Gamma_{R1} \Gamma_{L;22}$, $\Gamma_{L;11} \Gamma_{R2}$, and $\Gamma_{R1} \Gamma_{R2}$ can make a triangle, or

$$|\Gamma_{R1} \Gamma_{L;22} - \Gamma_{L;11} \Gamma_{R2}| < \Gamma_{R1} \Gamma_{R2} < \Gamma_{R1} \Gamma_{L;22} + \Gamma_{L;11} \Gamma_{R2} \quad (\text{A}\cdot 13)$$

is satisfied. This condition is usually realized if the Γ 's are in the same order of magnitude.

Appendix B: Hamiltonian in Space of Many-Body States

In the presence of U , we diagonalize the effective Hamiltonian $H_{\text{eff}}^{\text{DQD}}$ in Eq. (8) in the space of many-body states in the DQD. The Hamiltonian is block-diagonalized into three subspaces with the total spin of $S = 0, 1/2$, and 1.

For spin singlet ($S = 0$), there are five states, $|0\rangle$, $|s\rangle$ in Eq. (18), $|1 \uparrow, 1 \downarrow\rangle$, $|2 \uparrow, 2 \downarrow\rangle$, and $|1 \uparrow, 1 \downarrow, 2 \uparrow, 2 \downarrow\rangle$. Using these states as a basis set, the Hamiltonian is represented by

$$\begin{pmatrix} 0 & \sqrt{2}\Gamma_{\text{CAR}}^* & \Gamma_{\text{LAR},1}^* & \Gamma_{\text{LAR},2}^* & 0 \\ \sqrt{2}\Gamma_{\text{CAR}} & \varepsilon_1 + \varepsilon_2 & 0 & 0 & -\sqrt{2}\Gamma_{\text{CAR}}^* \\ \Gamma_{\text{LAR},1} & 0 & 2\varepsilon_1 + U & 0 & \Gamma_{\text{LAR},2}^* \\ \Gamma_{\text{LAR},2} & 0 & 0 & 2\varepsilon_2 + U & \Gamma_{\text{LAR},1}^* \\ 0 & -\sqrt{2}\Gamma_{\text{CAR}} & \Gamma_{\text{LAR},2} & \Gamma_{\text{LAR},1} & 2(\varepsilon_1 + \varepsilon_2 + U) \end{pmatrix}. \quad (\text{B}\cdot 1)$$

When $U = 0$, the eigenenergies of Eq. (B.1) are $\varepsilon_1 + \varepsilon_2 \pm E_1 \pm E_2$ and $\varepsilon_1 + \varepsilon_2$, where E_1 and E_2 are the eigenenergies of the BdG equation in Sect. A.1. The lowest energy, $\varepsilon_1 + \varepsilon_2 - E_1 - E_2$, coincides with E_{GS} in Eq. (14). If the groundstate is denoted by $|\text{GS}\rangle$, the other states are written as $\gamma_{1\uparrow}^\dagger \gamma_{1\downarrow}^\dagger |\text{GS}\rangle$, $\gamma_{2\uparrow}^\dagger \gamma_{2\downarrow}^\dagger |\text{GS}\rangle$, $\gamma_{1\uparrow}^\dagger \gamma_{1\downarrow}^\dagger \gamma_{2\uparrow}^\dagger \gamma_{2\downarrow}^\dagger |\text{GS}\rangle$, and $(\gamma_{1\uparrow}^\dagger \gamma_{2\downarrow}^\dagger - \gamma_{1\downarrow}^\dagger \gamma_{2\uparrow}^\dagger) |\text{GS}\rangle / \sqrt{2}$.

For spin doublet ($S = 1/2$), there are four states, $|1 \uparrow\rangle$, $|2 \uparrow\rangle$, $|1 \uparrow, 2 \uparrow, 2 \downarrow\rangle$, $|1 \uparrow, 1 \downarrow, 2 \uparrow\rangle$, with $S_z = 1/2$, and four states, $|1 \downarrow\rangle$, $|2 \downarrow\rangle$, $|1 \downarrow, 2 \uparrow, 2 \downarrow\rangle$, $|1 \uparrow, 1 \downarrow, 2 \downarrow\rangle$, with $S_z = -1/2$. The representation matrix of the Hamiltonian is given by

$$\begin{pmatrix} \varepsilon_1 & 0 & \Gamma_{\text{LAR},2}^* & -\Gamma_{\text{CAR}}^* \\ 0 & \varepsilon_2 & -\Gamma_{\text{CAR}}^* & \Gamma_{\text{LAR},1}^* \\ \Gamma_{\text{LAR},2} & -\Gamma_{\text{CAR}} & \varepsilon_1 + 2\varepsilon_2 + U & 0 \\ -\Gamma_{\text{CAR}} & \Gamma_{\text{LAR},1} & 0 & 2\varepsilon_1 + \varepsilon_2 + U \end{pmatrix} \quad (\text{B}\cdot 2)$$

for both $S_z = 1/2$ and $-1/2$. When $U = 0$, the eigenenergies are $\varepsilon_1 + \varepsilon_2 \pm E_1$ and $\varepsilon_1 + \varepsilon_2 \pm E_2$.

The eigenstates are $\gamma_{1\sigma}^\dagger|\text{GS}\rangle$, $\gamma_{2\sigma}^\dagger|\text{GS}\rangle$, $\gamma_{1\sigma}^\dagger\gamma_{2\uparrow}^\dagger\gamma_{2\downarrow}^\dagger|\text{GS}\rangle$, and $\gamma_{1\uparrow}^\dagger\gamma_{1\downarrow}^\dagger\gamma_{2\sigma}^\dagger|\text{GS}\rangle$ with $\sigma = \uparrow$ or \downarrow .

For spin triplet ($S = 1$), there are three states, $|1 \uparrow, 2 \uparrow\rangle$, $|t\rangle$ in Eq. (19), and $|1 \downarrow, 2 \downarrow\rangle$. They are eigenstates of the Hamiltonian with eigenenergy $\varepsilon_1 + \varepsilon_2$ even in the presence of U . They are given by $\gamma_{1\uparrow}^\dagger\gamma_{2\uparrow}^\dagger|\text{GS}\rangle$, $\gamma_{1\downarrow}^\dagger\gamma_{2\downarrow}^\dagger|\text{GS}\rangle$, and $(\gamma_{1\uparrow}^\dagger\gamma_{2\downarrow}^\dagger + \gamma_{1\downarrow}^\dagger\gamma_{2\uparrow}^\dagger)|\text{GS}\rangle/\sqrt{2}$, where $|\text{GS}\rangle$ is the spin-singlet groundstate in the absence of U .

Appendix C: Single QD with Three Superconducting Leads

Here, we examine a single QD connected to three superconducting leads, as depicted in Fig. 1(b). By the same procedure as in Sect. 2.1, we derive the effective Hamiltonian,

$$H_{\text{eff}}^{\text{QD}} = H_{\text{dot}} + H_{\text{AR}} \quad (\text{C}\cdot 1)$$

with

$$H_{\text{dot}} = \sum_{\sigma} \varepsilon_0 d_{\sigma}^{\dagger} d_{\sigma} + U n_{\uparrow} n_{\downarrow}, \quad (\text{C}\cdot 2)$$

$$H_{\text{AR}} = \Gamma_{\text{AR}} d_{\uparrow}^{\dagger} d_{\downarrow}^{\dagger} + \text{h.c.}, \quad (\text{C}\cdot 3)$$

where

$$\Gamma_{\text{AR}} = -\Gamma_0 e^{i\phi_0} - \Gamma_1 e^{i\phi_1} - \Gamma_2 e^{i\phi_2}. \quad (\text{C}\cdot 4)$$

Here, ε_0 and U are the energy level and electron-electron interaction in the QD, respectively. $n_{\sigma} = d_{\sigma}^{\dagger} d_{\sigma}$ is the number operator with spin σ in the QD. Γ_j is the level broadening due to the tunnel coupling to lead j , which is defined by a similar equation to Eq. (5). ϕ_j is the superconducting phase in lead j . We introduce the phase differences $\varphi_1 = \phi_0 - \phi_1$ and $\varphi_2 = \phi_0 - \phi_2$.

C.1 In case of $U = 0$

We begin with the case of $U = 0$. The energies of the Andreev bound states are $\pm E_1$, where

$$E_1 = \sqrt{\varepsilon_0^2 + |\Gamma_{\text{AR}}|^2}. \quad (\text{C}\cdot 5)$$

The groundstate energy is given by $E_{\text{GS}} = -E_1 + \varepsilon_0$. The supercurrent to lead j ($= 1, 2$) is obtained by

$$I_j(\varphi_1, \varphi_2) = \frac{2e}{\hbar} \frac{\partial E_{\text{GS}}}{\partial \varphi_j} = -\frac{2e}{\hbar} \frac{\partial E_1}{\partial \varphi_j} \quad (\text{C}\cdot 6)$$

at $T = 0$.

Let us examine E_1 in Eq. (C·5). $|\Gamma_{\text{AR}}|^2$ is rewritten as

$$\begin{aligned} |\Gamma_{\text{AR}}|^2 = & \Gamma_0^2 + \Gamma_1^2 + \Gamma_2^2 + 2\Gamma_0\Gamma_2 \cos \varphi_2 \\ & + 2\Gamma_1 \sqrt{\Gamma_0^2 + \Gamma_2^2 + 2\Gamma_0\Gamma_2 \cos \varphi_2} \cos(\varphi_1 - \Phi), \end{aligned} \quad (\text{C}\cdot 7)$$

where Φ is given by

$$\cos \Phi = \frac{\Gamma_0 + \Gamma_2 \cos \varphi_2}{\sqrt{\Gamma_0^2 + \Gamma_2^2 + 2\Gamma_0\Gamma_2 \cos \varphi_2}}, \quad (\text{C}\cdot 8)$$

$$\sin \Phi = \frac{\Gamma_2 \sin \varphi_2}{\sqrt{\Gamma_0^2 + \Gamma_2^2 + 2\Gamma_0\Gamma_2 \cos \varphi_2}}. \quad (\text{C}\cdot 9)$$

For a given φ_2 , the groundstate energy E_{GS} is the minimum at $\varphi_1 = \Phi$. As a result, the supercurrent I_1 flows at $\varphi_1 = 0$ unless $\Phi = 0, \pi$ or $\varphi_2 = 0, \pi$ (anomalous Josephson effect), as seen in Fig. C·1(e). Note that Φ can be controlled by φ_2 in this device.

Since E_{GS} is an even function of $(\varphi_1 - \Phi)$, the maximum and minimum of I_1 are identical in magnitude, $I_c^- = I_c^+$. Hence no SDE is observed.

We investigate the zero points of the energies of the Andreev bound states, $\pm E_1$ in Eq. (C·5). If $\varepsilon_0 = 0$, the solutions of $|\Gamma_{\text{AR}}| = 0$ exist when the triangle inequality

$$|\Gamma_1 - \Gamma_2| < \Gamma_0 < \Gamma_1 + \Gamma_2 \quad (\text{C}\cdot 10)$$

is fulfilled.^{47,48)} Then, there are two solutions given by

$$\cos \varphi_1 = \frac{\Gamma_2^2 - \Gamma_1^2 - \Gamma_0^2}{2\Gamma_0\Gamma_1}, \quad (\text{C}\cdot 11)$$

$$\cos \varphi_2 = \frac{\Gamma_1^2 - \Gamma_2^2 - \Gamma_0^2}{2\Gamma_0\Gamma_2}, \quad (\text{C}\cdot 12)$$

$$\sin \varphi_2 = -\frac{\Gamma_1}{\Gamma_2} \sin \varphi_1. \quad (\text{C}\cdot 13)$$

When $\Gamma_0 = \Gamma_1 = \Gamma_2$, they are $(\varphi_1, \varphi_2) = (2\pi/3, -2\pi/3)$ and $(-2\pi/3, 2\pi/3)$.

When $\varepsilon_0 = 0$, we expand $E_1 = |\Gamma_{\text{AR}}|$ around a zero point, $(\varphi_1^{(0)}, \varphi_2^{(0)})$. For $\varphi_1 = \varphi_1^{(0)} + \delta\varphi_1$ and $\varphi_2 = \varphi_2^{(0)} + \delta\varphi_2$,

$$E_1 \simeq \sqrt{\Gamma_1^2 \cos^2 \theta + \Gamma_2^2 \sin^2 \theta - \frac{1}{2}(\Gamma_1^2 + \Gamma_2^2 - \Gamma_0^2) \sin 2\theta \delta\varphi}, \quad (\text{C}\cdot 14)$$

where $\delta\varphi_1 = \delta\varphi \cos \theta$ and $\delta\varphi_2 = \delta\varphi \sin \theta$ ($\delta\varphi > 0$). This indicates an anisotropic Dirac cone. When $\delta\varphi_2 = 0$ ($\theta = 0, \pi$), $E_1(\varphi_1^{(0)} \pm \delta\varphi, \varphi_2^{(0)}) \simeq \Gamma_1 \delta\varphi$, and thus $\partial E_1 / \partial \varphi_1 = \pm \Gamma_1$ at $\varphi_1 = \varphi_1^{(0)} \pm 0$ and $\varphi_2 = \varphi_2^{(0)}$.

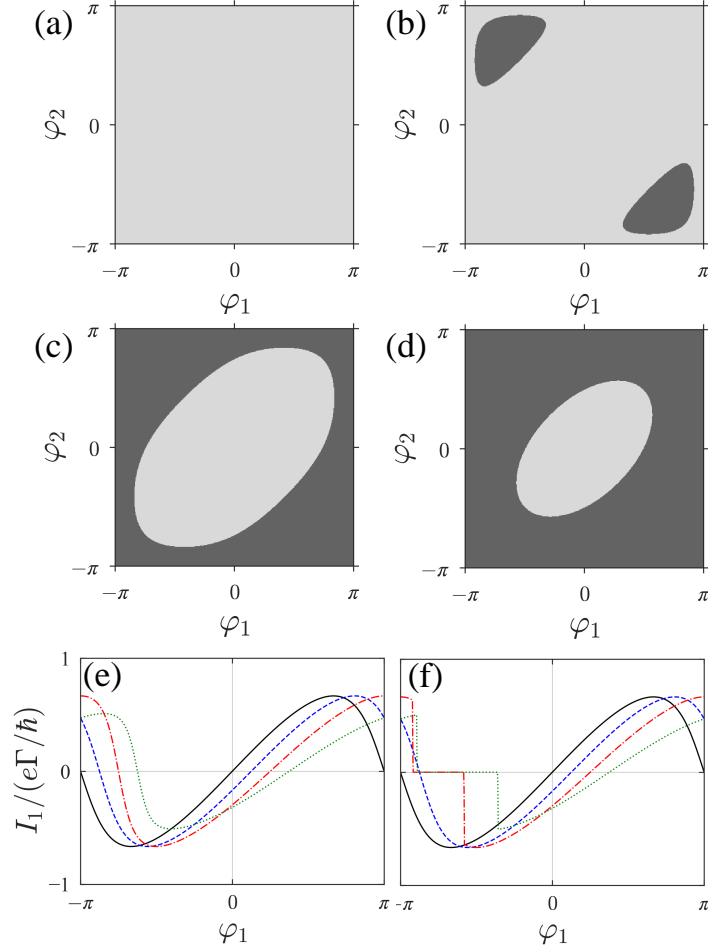


Fig. C.1. (Color online) (a)–(d) Spin of the groundstate and (e), (f) supercurrent I_1 to lead 1 in the model in Fig. 1(b). $\varepsilon_0 = -U/2$ and $\Gamma_0 = \Gamma_1 = \Gamma_2 \equiv \Gamma/3$. The spin singlet (doublet) regions are indicated by light gray (dark gray) in the $\varphi_1 - \varphi_2$ plane for (a) $U/\Gamma = 0$, (b) 0.5, (c) 1, and (d) 1.5. The supercurrent I_1 is plotted as a function of φ_1 when φ_2 is fixed at 0 (solid line), $\pi/4$ (broken line), $\pi/2$ (dash-dotted line), and $3\pi/4$ (dotted line), for (e) $U/\Gamma = 0$ and (f) 0.5. In panel (f), $I_1 = 0$ in the doublet region.

C.2 In case of $U \neq 0$

In the presence of U , the groundstate is spin singlet or doublet in the device of single QD. We rewrite H_{dot} in Eq. (C.2) as

$$H_{\text{dot}} = \sum_{\sigma} \xi_0 d_{\sigma}^{\dagger} d_{\sigma} + \frac{U}{2} \left(\sum_{\sigma} n_{\sigma} - 1 \right)^2 - \frac{U}{2}, \quad (\text{C.15})$$

where $\xi_0 = \varepsilon_0 + (U/2)$. For the spin-singlet states, which are given by linear combinations of $|0\rangle$ and $|\uparrow, \downarrow\rangle$, the second and third terms are cancelled with each other on the right side of Eq. (C.15). The lowest energy is

$$E_{\text{singlet}}(\varphi_1, \varphi_2) = -\sqrt{\xi_0^2 + |\Gamma_{\text{AR}}|^2} + \xi_0 \quad (\text{C.16})$$

with Γ_{AR} in Eq. (C·4). This equation is just obtained by replacing ε_0 with ξ_0 in the groundstate energy for $U = 0$.²³⁾

The spin-doublet states ($|\uparrow\rangle, |\downarrow\rangle$) have the energy of $E_{\text{doublet}} = \varepsilon_0 = \xi_0 - (U/2)$ since H_{AR} is irrelevant in $H_{\text{eff}}^{\text{QD}}$ in Eq. (C·1). In the doublet phase, no supercurrent flows because E_{doublet} does not depend on φ_1 .

The groundstate energy E_{GS} is determined by the minimum between E_{singlet} and E_{doublet} . In Figs. C·1(a)–(d), we show the phase diagram of the single QD in the $\varphi_1 - \varphi_2$ plane for several values of U . We set $\xi_0 = 0$. The singlet phase always appears for $U = 0$ while both singlet and doublet phases are seen for $U \neq 0$.

Fixing at $\xi_0 = 0$, we evaluate the supercurrent to lead 1, I_1 , using the first equation in Eq. (C·6). In Figs. C·1(e) and (f), the supercurrent I_1 is depicted as a function of φ_1 for a given φ_2 when (e) $U = 0$ and (f) $U/\Gamma = 0.5$ with $\Gamma = \Gamma_0 + \Gamma_1 + \Gamma_2$. In the presence of U , the current is equivalent to that for $U = 0$ in the singlet phase, whereas $I_1 = 0$ in the doublet phase.

References

- 1) F. Ando, Y. Miyasaka, T. Li, J. Ishizuka, T. Arakawa, Y. Shiota, T. Moriyama, Y. Yanase, and T. Ono, *Nature* **584**, 373 (2020).
- 2) L. Hu, C. Wu, and X. Dai, *Phys. Rev. Lett.* **99**, 067004 (2007).
- 3) A. A. Reynoso, G. Usaj, C. A. Balseiro, D. Feinberg, and M. Avignon, *Phys. Rev. Lett.* **101**, 107001 (2008).
- 4) A. Zazunov, R. Egger, T. Jonckheere, and T. Martin, *Phys. Rev. Lett.* **103**, 147004 (2009).
- 5) T. Yokoyama, M. Eto, and Yu. V. Nazarov, *J. Phys. Soc. Jpn.* **82**, 054703 (2013).
- 6) T. Yokoyama, M. Eto, and Yu. V. Nazarov, *Phys. Rev. B* **89**, 195407 (2014).
- 7) C. Baumgartner, L. Fuchs, A. Costa, S. Reinhardt, S. Gronin, G. C. Gardner, T. Lindemann, M. J. Manfra, P. E. Faria, Jr., D. Kochan, J. Fabian, N. Paradiso, and C. Strunk, *Nat. Nanotechnol.* **17**, 39 (2022).
- 8) H. Wu, Y. Wang, Y. Xu, P. K. Sivakumar, C. Pasco, U. Filippozzi, S. S. P. Parkin, Y.-J. Zeng, T. McQueen, and M. N. Ali, *Nature* **604**, 653 (2022).
- 9) B. Pal, A. Chakraborty, P. K. Sivakumar, M. Davydova, A. K. Gopi, A. K. Pandeya, J. A. Krieger, Y. Zhang, M. Date, S. Ju, N. Yuan, N. B. M. Schröter, L. Fu, and S. S. P. Parkin, *Nat. Phys.* **18**, 1228 (2022).
- 10) A. Costa, C. Baumgartner, S. Reinhardt, J. Berger, S. Gronin, G. C. Gardner, T. Lindemann, M. J. Manfra, J. Fabian, D. Kochan, N. Paradiso, and C. Strunk, *Nat. Nanotechnol.* **18**, 1266 (2023).
- 11) A. Banajee, M. Geier, M. A. Rahman, C. Thomas, T. Wang, M. J. Manfra, K. Flensberg, and C. M. Marcus, *Phys. Rev. Lett.* **131**, 196301 (2023).
- 12) C. Ciaccia, R. Haller, A. C. C. Drachmann, T. Lindemann, M. J. Manfra, C. Schrade, and C. Schrönenberger, *Phys. Rev. Res.* **5**, 033131 (2023).
- 13) A. Greco, Q. Pichard, and F. Giazotto, *Appl. Phys. Lett.* **123**, 092601 (2023).
- 14) M. Gupta, G. V. Graziano, M. Pendharkar, J. T. Dong, C. P. Dempsey, C. Palmstrøm, and V. S. Pribiag, *Nat. Commun.* **14**, 3078 (2023).
- 15) M. Coraiola, D. Z. Haxwell, D. Sabonis, H. Weisbrich, A. E. Svetogorov, M. Hinderling, S. C. ten Kate, E. Cheah, F. Krizek, R. Schott, W. Wegscheider, J. C. Cuevas, W. Belzig, and F. Nichele, *Nat. Commun.* **14**, 6784 (2023).

- 16) S. Matsuo, T. Imoto, T. Yokoyama, Y. Sato, T. Lindemann, S. Gronin, G. C. Gardner, M. J. Manfra, and S. Tarucha, *Nat. Phys.* **19**, 1636 (2023).
- 17) S. Matsuo, T. Imoto, T. Yokoyama, Y. Sato, T. Lindemann, S. Gronin, G. C. Gardner, M. J. Manfra, and S. Tarucha, *Sci. Adv.* **9**, eadj3698 (2023).
- 18) V. Kornich, H. S. Barakov, and Yu. V. Nazarov, *Phys. Rev. Res.* **1**, 033004 (2019).
- 19) V. Kornich, H. S. Barakov, and Yu. V. Nazarov, *Phys. Rev. B* **101**, 195430 (2020).
- 20) S. Matsuo, J. S. Lee, C.-Y. Chang, Y. Sato, K. Ueda, C. J. Palmstrøm, and S. Tarucha, *Commun Phys.* **5**, 221 (2022).
- 21) J.-D. Pillet, S. Annabi, A. Peugeot, H. Riechert, E. Arrighi, J. Griesmar, and L. Bretheau, *Phys. Rev. Res.* **5**, 033199 (2023).
- 22) S. Matsuo, T. Imoto, T. Yokoyama, Y. Sato, T. Lindemann, S. Gronin, G. C. Gardner, S. Nakosai, Y. Tanaka, M. J. Manfra, and S. Tarucha, *Nat. Commun.* **14**, 8271 (2023).
- 23) V. Meden, *J. Phys.: Condens. Matter* **31**, 163001 (2019).
- 24) J. A. van Dam, Yu. V. Nazarov, E. P. A. M. Bakkers, S. De Franceschi, and L. P. Kouwenhoven, *Nature* **442**, 667 (2006).
- 25) M.-S. Choi, C. Bruder, and D. Loss, *Phys. Rev. B* **62**, 13569 (2000).
- 26) H. Pan and T.-H. Lin, *Phys. Rev. B* **74**, 235312 (2006).
- 27) Z. Wang and X. Hu, *Phys. Rev. Lett.* **106**, 037002 (2011).
- 28) P. Recher, E. V. Sukhorukov, and D. Loss, *Phys. Rev. B* **63**, 165314 (2001).
- 29) R. S. Deacon, A. Oiwa, J. Sailer, S. Baba, Y. Kanai, K. Shibata, K. Hirakawa, and S. Tarucha, *Nat. Commun.* **6**, 7446 (2015).
- 30) M Leijnse and K. Flensberg, *Phys. Rev. B* **86**, 134528 (2012).
- 31) T. Dvir, G. Wang, N. van Loo, C.-X. Liu, G. P. Mazur, A. Bordin, S. L. D. ten Haaf, J.-Y. Wang, D. van Driel, F. Zatelli, X. Li, F. K. Malinowski, S. Gazibegovic, G. Badawy, E. P. A. M. Bakkers, M. Wimmer, and L. P. Kouwenhoven, *Nature* **614**, 445 (2023).
- 32) A. Bordin, G. Wang, C.-X. Liu, S. L. D. ten Haaf, N. van Loo, G. P. Mazur, D. Xu, D. van, Driel, F. Zatelli, S. Gazibegovic, G. Badawy, E. P. A. M. Bakkers, M. Wimmer, L. P. Kouwenhoven, and T. Dvir, *Phys. Rev. X* **13**, 031031 (2023).
- 33) T. Yokoyama and Yu. V. Nazarov, *Phys. Rev. B* **92**, 155437 (2015).
- 34) R.-P. Riwar, M. Houzet, J. S. Meyer, and Yu. V. Nazarov, *Nat. Commun.* **7**, 11167 (2016).

- 35) R. L. Klees, G. Rastelli, J. C. Cuevas, and W. Belzig, Phys. Rev. Lett. **124**, 197002 (2020).
- 36) Q. Cheng and Q.-F. Sun, Phys. Rev. B **107**, 184511 (2023).
- 37) D. Debnath and P. Dutta, Phys. Rev. B **109**, 174511 (2024).
- 38) T. Kubo, Y. Tokura, T. Hatano, and S. Tarucha, Phys. Rev. B **74**, 205310 (2006).
- 39) Y. Zhang, R. Sakano, and M. Eto, J. Phys. Soc. Jpn. **91**, 014703 (2022).
- 40) Y. Zhang, M. Kato, R. Sakano, and M. Eto, J. Phys. Soc. Jpn. **93**, 024702 (2024).
- 41) M. Eto and R. Sakano, Phys. Rev. B **102**, 245402 (2020).
- 42) S. Bravyi, D. P. DiVincenzo, and D. Loss, Ann. Phys. **326**, 2793 (2011).
- 43) Z. Scherübl, A. Pályi, and S. Csonka, Beilstein J. Nanotechnol. **10**, 363 (2019).
- 44) M. Spethmann, S. Bosco, A. Hofmann, J. Klinovaja, and D. Loss, Phys. Rev. B **109**, 085303 (2024).
- 45) Our numerical study indicates that φ_2 at the Dirac points almost coincides with φ_2 at the maximum of I_c^\pm when $|\varepsilon_0|/\Gamma \lesssim 0.4$.
- 46) T. Meng and S. Florens, and P. Simon, Phys. Rev. B **79**, 224521 (2009).
- 47) P. Zalom, M. Žonda, and T. Novotný, Phys. Rev. Lett. **132**, 126505 (2024).
- 48) In the two-terminal geometry ($\Gamma_2 = 0$), the energies of Andreev bound state have a zero point when $\varepsilon_0 = 0$ and $\Gamma_1 = \Gamma_2$. Regarding the condition for Γ 's, the zero points are easily realized in the three-terminal geometry.